ChemComm
Chemical Communications

Accepted Manuscript

This article can be cited before page numbers have been issued, to do this please use: T. Wang, M. Fu, H. Wang, C. Yi, D. Chen, Q. Liu, Y. Meng, J. Hu and T. Liu, *Chem. Commun.*, 2026, DOI: 10.1039/D6CC02265K.

ROYAL SOCIETY OF CHEMISTRY

rsc.li/chemcomm

View Article Online
DOI: 10.1039/D6CC02265K

ARTICLE

Intermediate Single Crystal Trapping of COF-300 via Organic Lewis Acid Catalysis

Received 00th January 20xx,
Accepted 00th January 20xx

DOI: 10.1039/x0xx00000x

Tian Wang[+a], Ming-Yang Fu[+a], Hao Wang [+a], Cheng Yi [a], Du-Yong Chen [a], Qiang Liu [a], Yin-Shan Meng [a, c], Jiyun Hu*[b], Tao Liu*[a, c]

A sterically hindered organic Lewis acid catalyst $B(C_6F_5)_3$ was utilized to regulate the reaction kinetics of COF-300 synthesis, enabling direct observation of the intermediate single-crystal growth stage. This approach establishes a novel experimental basis for mechanistic studies of COFs crystallization and provides valuable insight into controlled crystal formation pathways.

Covalent organic frameworks (COFs) are crystalline porous materials formed through the covalent bonding extension of organic building blocks.[1, 2] The vast reticular chemical design space imparts substantial versatility in the structures and functions of COFs.[3-8] A long-standing issue in COF chemistry is the understanding and control of the crystallization process. Traditional solvothermal synthesis is typically subjected to uncontrolled polymerization, where fast precipitation of polymers occurs, leading to powder COFs with small crystal domains.[9] Single crystals are crucial for precise structural characterization, enabling deeper insights into structure–property correlations that are otherwise obscured by the limitations inherent to powder samples.[10-14] The breakthroughs in the controlled growth of COFs were achieved in 2018. Dichtel's team obtained large boronate ester–linked 2D COF single crystals by slowly adding monomers to preformed nanoparticle seed colloids.[15] Ma and coworkers successfully synthesized single crystals of imine-linked 3D COFs using a modulated approach.[10]

Despite the significant progress in synthesizing single-crystalline COFs, further controlling the growth process and investigating the involved intermediate phases are challenging.[16, 17] Lotsch and coworkers observed a solvated triple imine condensation product of 1,3,5-triformylbenzene intermediate during mechanochemical synthesis of LZU-1.[18] Ma and coworkers synthesized an imine oligomer of COF-320 via a liquid-liquid interfacial crystallization method.[19] Wang and colleagues prepared similar imine-linked oligomers using ionic liquids as a catalyst.[20] We reason that the steric hindrance of the catalyst may provide an additional way to regulate the polymerization degree in COF synthesis.[21] In this work, we show that $B(C_6F_5)_3$ (BCF), a classical bulky organic Lewis acid, can promote both the formation of oligomer intermediate and final framework of COF-300 under carefully controlled conditions (Scheme 1).[22, 23]

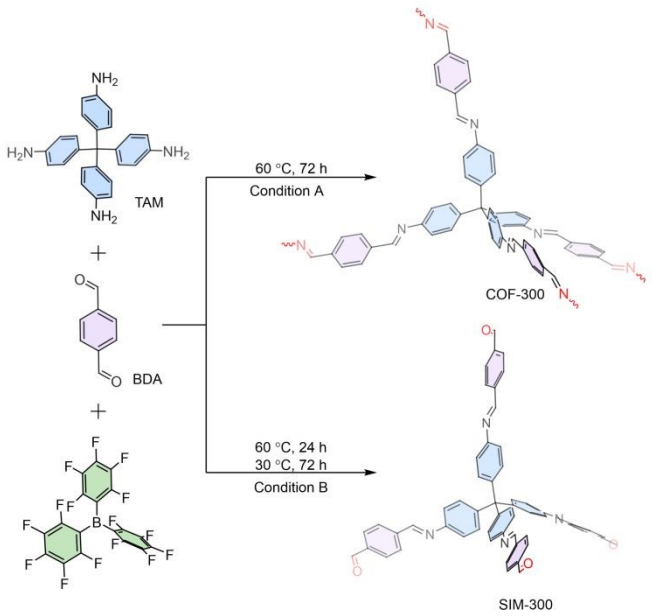

Scheme 1. Synthesis of COF-300 and SIM-300.

The condensation of tetrakis(4-aminophenyl)methane (TAM) and 1,4-benzenedialdehyde (BDA) in 2 mL 1,4-dioxane/mesitylene (1/3, v/v) with a catalytic amount of BCF at 60 °C for 72 h yields the 7-fold interpenetrated hydrated COF-300 (Scheme 1, condition A).[11, 24] The Powder X-ray diffraction (PXRD) pattern (Figure 1a) and the characteristic C=N stretching vibration at 1621 cm^{-1} in the FT-IR spectrum matches the reported data of COF-300 (Figure 1b).[24] The COF-300 produced by this method has a high Brunauer-Emmett-Teller (BET) surface area of 956 $m^2\ g^{-1}$ (Figure 1c) and is thermally stable up to 400 °C (Figure S1).

[a] State Key Laboratory of Fine Chemicals, Frontier Science Center for Smart Materials, School of Chemical Engineering, Dalian University of Technology, No.2 Linggong Road, Dalian 116024, China; E-mail: mengys@dlut.edu.cn; liutao@dlut.edu.cn.
[b] Dongguan Key Laboratory of Interdisciplinary Science for Advanced Materials and Large-Scale Scientific Facilities, School of Physical Sciences, Great Bay University, Dongguan 523000, China. E-mail: hujiyun@gbu.edu.cn
[c] Liaoning Binhai Laboratory, Dalian 116023, China.
[+] Tian Wang, Ming-Yang Fu and Hao Wang contributed equally to this work.

In contrast, when incubating the reaction mixture at 30 °C for 72 h after the initial reaction at 60 °C for 24 h, yellow single crystals of the intermediate oligomer SIM-300 were obtained (Scheme 1, condition B).[23] The PXRD pattern of SIM-300 is significantly different from that of COF-300, demonstrating its different phase structure (Figure 1a). The FT-IR spectrum of SIM-300 exhibits a strong vibration band at 1698 cm^{-1}, corresponding to the unreacted aldehyde group, in addition to the C=N vibration band at 1621 cm^{-1} (Figure 1b). Solid-state ^{13}C NMR spectroscopy confirms both the presence of aldehyde and imine groups in SIM-300, showing the corresponding signal at 192 and 157 ppm respectively (Figure 1d). The linker composition of SIM-300 determined by ^{1}H NMR spectroscopy after acid digestion matches the theoretical value of 1:4 (TAM to BDA, Figure S2). Nitrogen sorption study shows that SIM-300 is nonporous with a low BET surface area of 48 $m^2\ g^{-1}$ (Figure 1c). The thermogravimetric analysis (TGA) revealed that SIM-300 is thermally stable up to 400 °C under a nitrogen atmosphere (Figure S1).

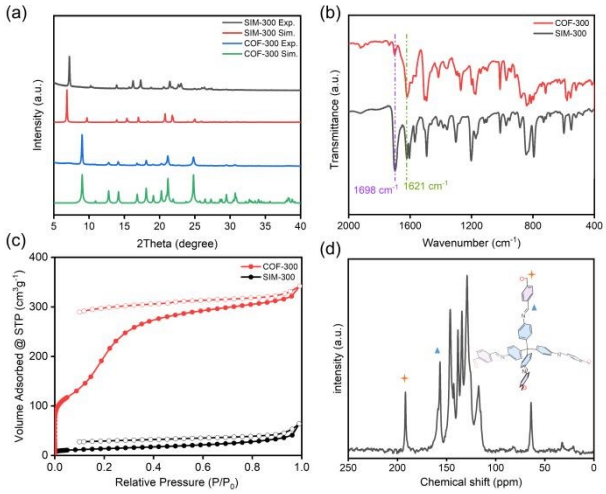

Figure 1. (a) Experimental and simulated PXRD patterns, (b) FT-IR spectra, and (c) N_2 sorption isotherms of COF-300 and SIM-300. (d) solid-state ^{13}C NMR spectra of SIM-300.

The structure of SIM-300 is unambiguously resolved by single-crystal X-ray diffraction analysis (Figure 2). SIM-300 crystallizes in the $I4_1/a$ space group with unit-cell parameters of a = b = 25.771(2) Å, c = 7.6244(8) Å, and α = β = γ = 90°. The oligomer molecule adopts a quasi-tetrahedral conformation, featuring four terminal, unreacted aldehyde groups positioned at the ends of its four arms. The oxygen atom of the aldehyde group forms an intramolecular O···H–C hydrogen bond with an adjacent molecule in the unit cell ($d_{O\cdots H}$ = 2.611 Å, Figure 2). These hydrogen-bond interactions contribute to the formation of a densely packed three-dimensional network. It should be noted that TAM and COF-300 crystallize in the same $I4_1/a$ space group. The lattice parameters are a = b = 16.8018 Å, c = 7.1674 Å for TAM, and a = b = 26.2260(18) Å, c = 7.5743(10) Å for COF-300 respectively (Figure 3a).[10, 25] The central carbons of TAM entities in the unit cells of the three crystals locate at the same positions due to the symmetry constraints of $I4_1/a$ space group. Therefore, the molecular packings of the three crystals are also highly similar. The attachment of four BDA molecules to TAM via an imine bond leads to the formation of SIM, resulting in a remarkable expansion of the a and b axes from 16.8018 to 25.771(2) Å (53.4%) and a slight elongation of the c axis from 7.1674 to 7.6244(8) Å (6.4%) due to increased molecular size (Figure 3a). From SIM-300 to COF-300, a pair of oligomers related by (0, -0.5, 1.75) needs to expel one of the BDA fragments by breaking one C=N bond and then forming a new C=N bond between the released amine group and the aldehyde group of the other BDA fragment (Figure 3b and S3). This reorganization step only slightly changes the cell axis lengths from SIM-300 to COF-300 (< 2%, Figure 3a). The most influential structure features are the orientation of TAM and the dihedral angles between the two phenyl groups stretching to the c direction of TAM. In the crystal structure of SIM-300, the angles are 97.0 and 116.0° for one set of oligomer molecules and 108.8 and 109.8° for the other set (Figure S4). While in COF-300, the angles are 111.5° and 105.5° (Figure S5).

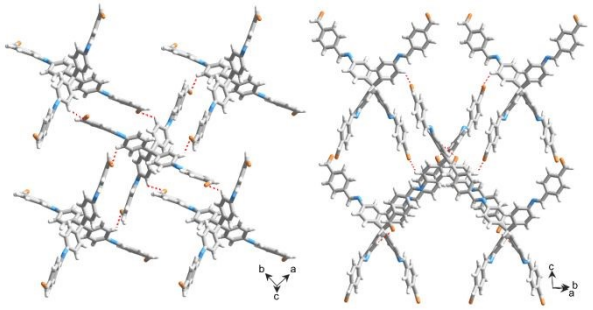

Figure 2. The single crystal structure of SIM-300 viewed from different directions.

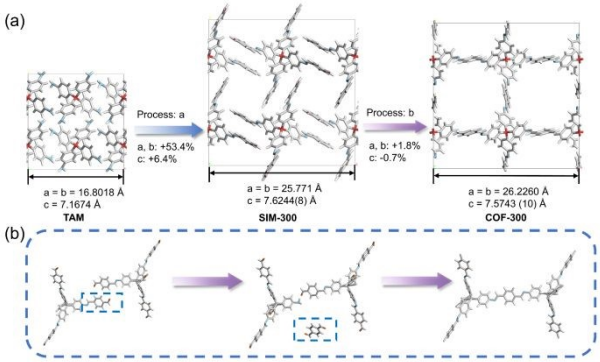

Figure 3. (a) The change of unit cell dimensions of from TAM to SIM-300, and to COF-300. (b) Schematic illustration of the structural transformation from SIM-300 to COF-300.

The distinct reaction pathways were further ex-situ investigated with scanning electron microscope (SEM) and PXRD analyses (Figure 4). For COF-300 growth under condition A, spherical aggregates consisting of elongated, rod-shaped crystallites were consistently observed throughout the reaction. As the reaction progressed, these aggregates became denser and the rod evolved with well-defined square-pyramidal ends (Figure 4a and S6). This morphological evolution is characteristic of an Ostwald ripening process.[26, 27] PXRD analysis revealed a SIM-300 to COF-300 transformation process. At 24 hours, characteristic diffraction peaks corresponding to SIM-300 were observed along with unreacted TAM. At 48 hours, a mixed phase containing both SIM-300 and COF-300 was detected. Finally, after 72 hours, sharp and distinct diffraction peaks

corresponding exclusively to COF-300 appeared (Figure 4c). Under condition B, visible grain-like microcrystals of SIM-300 began to appear after incubation at 30 °C for 24 hours, with significant disassembly of the initial spherical aggregates. In the next 48-72 hours, these crystals further grew to ca. 100 μm in size (Figure 4b). In the low temperature incubation stage, TAM was gradually consumed, and the diffraction intensity of SIM-300 became stronger with a smaller full width at half maximum, indicating increased crystal size (Figure 4d). This process is a typical Ostwald ripening process. The less stable spherical aggregates gradually dissolved to release molecular building blocks, facilitating the continuous growth of larger, thermodynamically favored SIM-300 single crystals.

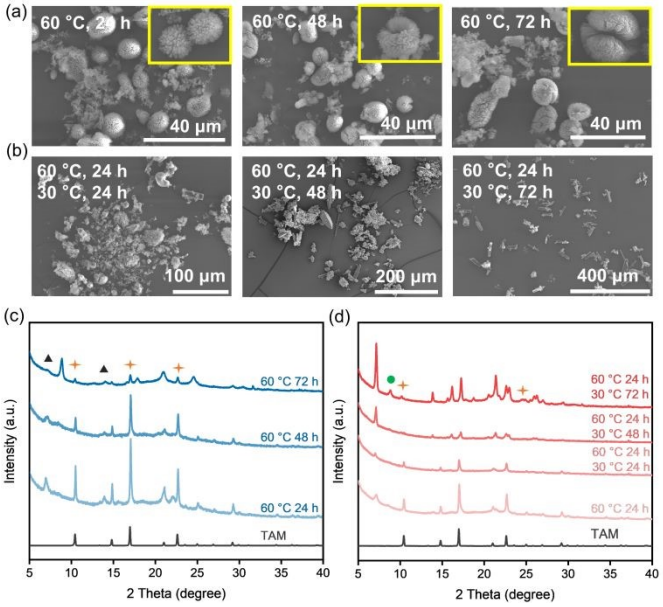

Figure 4. SEM images of solid precipitates at different time intervals during the synthesis of COF-300 (a) and SIM-300 (b). The corresponding PXRD patterns during the synthesis of COF-300 (c) and SIM-300 (d). Black triangles, orange asterisks, and green circles indicate the diffraction peaks of SIM-300, TAM, and COF-300, respectively.

To investigate differences in catalytic activity between AcOH and BCF, model Schiff base condensation reactions between benzaldehyde and aniline were conducted. As shown in Figure S7, the AcOH-catalyzed reaction rapidly approached equilibrium within 1 h (yield: 73%). In contrast, the BCF-catalyzed reaction achieved only a 57% yield after 1 h, which increased slightly to 70% after 3 h, indicating the lower catalytic activity of BCF. In addition to its weaker catalytic performance, the relatively large molecular size of BCF likely causes higher diffusion barriers to reactive sites compared to protons, thereby hindering further condensation or imine-exchange reactions, especially at lower temperatures. Consequently, BCF may become trapped within the initially formed dense SIM-300 network, restricting subsequent polymerization necessary for COF-300 formation. Under these conditions, SIM-300 crystals continue to grow via the Ostwald ripening process, ultimately yielding SIM-300 as a kinetically trapped product.

In summary, we have demonstrated that organic Lewis acid BCF can regulate the condensation kinetics in the synthesis of COF-300, enabling direct observation of the oligomer intermediate in single crystal form. SEM and PXRD monitoring of the reaction progress provide solid experimental evidence of a preassembly of oligomer intermediate and a subsequent phase transformation process during the formation of COF-300. This study complements the mechanistic understanding of COF growth proposed in recent intermediate tracing studies.[16, 28, 29] The approach presented herein offers an alternative approach for the controlled synthesis of COFs and an opportunity for investigating the crystallization dynamics of COFs.

This work was supported by the National Natural Science Foundation of China (Grants 22401035, 22025101, 22222103, 22173015), the Fundamental Research Funds for the Central Universities (DUT22LAB606), Liaoning Binhai Laboratory (LBLE-2023-02), and "Excellence Co-innovation Program" International Exchange Fund Project (DUTIO-ZG-202505), and Guangdong Basic and Applied Basic Research Foundation (2024A1515140058). J. H. thanks the startup fund from Great Bay University (YJKY230010) and Guangdong Recruitment Program (2023QN10C724) for support.

Conflicts of interest

The authors declare no competing financial interest.

Data availability

The data that support the findings of this study are available from the corresponding author upon reasonable request. CCDC 2512929 contains the supplementary crystallographic data for this paper. These data can be obtained free of charge via www.ccdc.cam.ac.uk/data_request/cif.

Notes and references

1. A. P. Côté, A. I. Benin, N. W. Ockwig, M. O'Keeffe, A. J. Matzger and O. M. Yaghi, *Science*, 2005, **310**, 1166-1170.
2. H. M. El-Kaderi, J. R. Hunt, J. L. Mendoza-Cortés, A. P. Côté, R. E. Taylor, M. O'Keeffe and O. M. Yaghi, *Science*, 2007, **316**, 268-272.
3. H. Zheng, H. Li, J. Ji, F. Chen, Y. Wang, J. Suo, J. Song, D. Zhao, V. Valtchev, S. Qiu and Q. Fang, *J. Am. Chem. Soc.*, 2025, **147**, 39223-39231.
4. J. Zhang, C. Cheng, L. Guan, H.-L. Jiang and S. Jin, *J. Am. Chem. Soc.*, 2023, **145**, 21974-21982.
5. W. Zhang, L. Chen, S. Dai, C. Zhao, C. Ma, L. Wei, M. Zhu, S. Y. Chong, H. Yang, L. Liu, Y. Bai, M. Yu, Y. Xu, X.-W. Zhu, Q. Zhu, S. An, R. S. Sprick, M. A. Little, X. Wu, S. Jiang, Y. Wu, Y.-B. Zhang, H. Tian, W.-H. Zhu and A. I. Cooper, *Nature*, 2022, **604**, 72-79.
6. H. S. Sasmal, A. Kumar Mahato, P. Majumder and R. Banerjee, *J. Am. Chem. Soc.*, 2022, **144**, 11482-11498.
7. X. Zhang, J. Hu, H. Liu, T. Sun, Z. Wang, Y. Zhao, Y.-B. Zhang, P. Huai, Y. Ma and S. Jiang, *J. Am. Chem. Soc.*, 2025, **147**, 1709-1720.
8. R. Liu, Z. Li, H. Zhao, L. Zhang, R. Lan, Q. Wang and H. Yang, *Adv. Funct. Mater.*, 2024, **35**.
9. B. J. Smith, A. C. Overholts, N. Hwang and W. R. Dichtel, *Chem. Commun.*, 2016, **52**, 3690-3693.

View Article Online
DOI: 10.1039/D6CC02265K

10. T. Ma, E. A. Kapustin, S. X. Yin, L. Liang, Z. Zhou, J. Niu, L.-H. Li, Y. Wang, J. Su, J. Li, X. Wang, W. D. Wang, W. Wang, J. Sun and O. M. Yaghi, *Science*, 2018, **361**, 48-52.
11. J. Han, J. Feng, J. Kang, J.-M. Chen, X.-Y. Du, S.-Y. Ding, L. Liang and W. Wang, *Science*, 2024, **383**, 1014-1019.
12. B. Yu, R.-B. Lin, G. Xu, Z.-H. Fu, H. Wu, W. Zhou, S. Lu, Q.-W. Li, Y. Jin, J.-H. Li, Z. Zhang, H. Wang, Z. Yan, X. Liu, K. Wang, B. Chen and J. Jiang, *Nat. Chem.*, 2024, **16**, 114-121.
13. J. Zhang, Z. Wang, J. Suo, C. Tuo, F. Chen, J. Chang, H. Zheng, H. Li, D. Zhang, Q. Fang and S. Qiu, *J. Am. Chem. Soc.*, 2024, **146**, 35090-35097.
14. L. Yi, Y. Gao, S. Luo, T. Wang and H. Deng, *J. Am. Chem. Soc.*, 2024, **146**, 19643-19648.
15. A. M. Evans, L. R. Parent, N. C. Flanders, R. P. Bisbey, E. Vitaku, M. S. Kirschner, R. D. Schaller, L. X. Chen, N. C. Gianneschi and W. R. Dichtel, *Science*, 2018, **361**, 52-57.
16. C. Kang, K. Yang, Z. Zhang, A. K. Usadi, D. C. Calabro, L. S. Baugh, Y. Wang, J. Jiang, X. Zou, Z. Huang and D. Zhao, *Nat. Commun.*, 2022, **13**, 1370.
17. W. Zhang, Y. Zhang, W. Ma, X. Han, W. Gong, Y. Liu and Y. Cui, *Chem*, 2025, **11**.
18. S. T. Emmerling, L. S. Germann, P. A. Julien, I. Moudrakovski, M. Etter, T. Friščić, R. E. Dinnebier and B. V. Lotsch, *Chem*, 2021, **7**, 1639-1652.
19. L. Hou, C. Shan, Y. Song, S. Chen, L. Wojtas, S. Ma, Q. Sun and L. Zhang, *Angew. Chem. Int. Ed.*, 2021, **60**, 14664-14670.
20. Z. Zheng, Q. Lin, S. Peng, Y. Zhang, S. Xu, H. Zhang and H. Wang, *Sci. China Chem.*, 2025, **68**, 3636-3646.
21. W. Zhao, Q. Zhu, X. Wu and D. Zhao, *Chem. Soc. Rev.*, 2024, **53**, 7531-7565.
22. F. J. Uribe-Romo, J. R. Hunt, H. Furukawa, C. Klöck, M. O'Keeffe and O. M. Yaghi, *J. Am. Chem. Soc.*, 2009, **131**, 4570-4571.
23. X. Shi, L. Yi and H. Deng, *Sci. China Chem.*, 2022, **65**, 1315-1320.
24. T. Ma, J. Li, J. Niu, L. Zhang, A. S. Etman, C. Lin, D. Shi, P. Chen, L.-H. Li, X. Du, J. Sun and W. Wang, *J. Am. Chem. Soc.*, 2018, **140**, 6763-6766.
25. D. Laliberté, T. Maris, E. Demers, F. Helzy, M. Arseneault and J. D. Wuest, *Cryst. Growth Des.*, 2005, **5**, 1451-1456.
26. W. Ma, G. Li, C. Zhong, Y. Yang, Q. Sun, D. Ouyang, W. Tong, W. Tian, L. Zhang and Z. Lin, *Chem. Commun.*, 2021, **57**, 7362-7365.
27. H. Zhao, G. Liu, Y. Liu, L. Zhou, L. Ma, Y. He, X. Zheng, J. Gao and Y. Jiang, *Nano Res.*, 2023, **16**, 281-289.
28. J. Liu, X. Su, Y. Xu, W. Tang, T. Yang and J. Gong, *Chem. Sci.*, 2025, **16**, 15037-15044.
29. L. Bourda, S. Bhandary, S. Ito, C. R. Göb, P. Van Der Voort, K. Van Hecke and L. Meshi, *IUCrJ*, 2024, **11**, 510-518.

View Article Online
DOI: 10.1039/D6CC02265K

The data that support the findings of this study are available from the corresponding author upon reasonable request. CCDC 2512929 contains the supplementary crystallographic data for this paper. These data can be obtained free of charge via www.ccdc.cam.ac.uk/data_request/cif.